Published by
NIGERIAN SOCIETY OF PHYSICAL SCIENCES
Available online @ https://journal.nsps.org.ng/index.php/jnsps

J. Nig. Soc. Phys. Sci. 8 (2026) 3353

Journal of the Nigerian Society of Physical Sciences

A hybrid process-based and neural network post-processing model for cowpea yield prediction under climate variability in North Central Nigeria

Onyeke Idoko Charles[a,*], John Kolo Alhassan[b], Mohammed Danlami Abdulmalik[b], Kehinde Dele Tolorunse[c]

[a]*Department of Computer Science, Joseph Sarwuan Tarka University, Makurdi, Nigeria*
[b]*Department of Computer Science, Federal University of Technology, Minna, Nigeria*
[c]*Department of Crop Production, Federal University of Technology, Minna, Nigeria*

Abstract

Agriculture has sustained human civilisation for centuries, yet it remains a sector in critical need of technological advancement. Existing crop-growth and yield-prediction methods lack a simple and generic framework that relies on climate data with minimal parameters, particularly for leguminous crops. Addressing this gap, this study develops a Crop Growth Rate Computation Model (CGRCM) to simulate crop growth with a focus on soil nitrogen utilisation. The CGRCM integrates climate variables and nine parameters to predict cowpea growth in terms of above-ground biomass and final yield, derived from biomass at maturity and harvest index. Climatic input data and soil parameters were obtained through remote sensing for Makurdi and Mokwa in North Central Nigeria, covering 32 growing seasons (1990–2021). The model was calibrated for the FUAMPEA cultivar and implemented using a Python-based neural network post-processor. Training was conducted on data from 1990–2017 and testing on data from 2018–2021. Results show that the CGRCM effectively captures biomass responses to drought, temperature and heat stress. The model achieved strong agreement with observed yields, with an MAE of 134.2, an RMSE of 153.6 and a prediction accuracy of 91.4% for Makurdi, and an MAE of 109.4, an RMSE of 113.7 and a prediction accuracy of 93.5% for Mokwa. Bootstrap confidence interval, paired *t*-test and Diebold–Mariano tests confirmed that the CGRCM performed better, demonstrating its reliability as a scalable and data-efficient tool for crop-growth prediction.

DOI: 10.46481/jnsps.2026.3353

Keywords: Climate, crop growth, yield prediction, neural network

Article History:
Received: 10 March 2026
Received in revised form: 01 May 2026
Accepted for publication: 12 May 2026
Available online: 19 May 2026

Communicated by: S. Folorunso

1. Introduction

Over the years, agriculture has supported the growth of human societies. However, it is among the numerous fields that urgently require technical assistance. The agricultural sector may not have entirely benefited from the latest technology, such as the Internet of Things (IoT). Through the application of intelligent monitoring techniques and the facilitation of automatic sensing for farm situations, a farmer can guarantee optimal production and yield by ensuring that the most effective methods are employed on their farm [1]. Environmental change is affecting both food and agricultural production. Variability in rainfall patterns and temperature swings has a negative impact on

*Corresponding Author Tel.: +2348038710118;
Email address: onyeke.idoko@uam.edu.ng (Onyeke Idoko Charles)

crop output, leading to reduced yields. Crop models have been widely used to evaluate the effects of climate change on crop growth [2].

Recently, there have been notable innovations in the application of machine learning across a range of fields and studies. Systems that apply machine learning to agriculture can also be developed for the benefit of the farming community [3]. Farmers are able to make intelligent choices regarding crop planting, watering and harvesting, thanks to machine learning, whose main goal is to maximise agricultural yield and reduce waste [4]. Menon *et al.* [5] suggested a system that forecasts crop conditions, suggests suitable remedies and identifies what crops need to be grown based on real-time data. It also follows field circumstances using climate analysis and detects large-scale crop diseases using decision trees. Worrall *et al.* [6] demonstrated how to use a domain-guided neural network (DgNN) to integrate agronomic understanding of agricultural growth factors into seasonal crop-growth appraisal. Geng *et al.* [7] proposed an enhanced system for modelling soil that incorporates data on crop-growth changes and machine-learning techniques. The authors highlighted the key benefits of including crop-growth characteristics based on remote sensing in soil-feature inversion during crop-covered scenarios and provided valuable information for computerised soil mapping.

Crop growth is frequently simulated using flexible crop models, but because these models are typically complicated, they have problems with parameter non-identifiability [8]. To achieve the goal of training one system for multiple cultivars, Li *et al.* [9] developed a Vision and Sensor Transformer (ViST) for crop-growth prediction by combining data from images and sensors. Kumar *et al.* [10] presented an intelligent system for tracking the progress and growth of leafy crops and providing real-time status reports. Using IoT, image processing and machine-learning technology, the approach was an innovative method to track the growth of leafy crops and provide real-time updates on their condition. Grindstaff *et al.* [11] created a system that uses Raspberry Pi devices to track plant development in buildings at a reasonable cost.

Previous studies have proposed a number of methods to address crop-growth prediction. Nevertheless, these methods were not sufficiently robust to present a simple, unified and generic model that is based on climate data and has few parameters for predicting the growth rate of all crop types, especially leguminous crops. Most of the research is focused on monitoring the impact of uncertainties from climate change on crop growth without considering nutrient utilisation, which also affects crop growth. To fill this gap, this study develops a hybrid crop-growth and yield-prediction framework that combines a neural network post-processor with a process-based crop growth rate computation model, using the basic environmental variables that account for crop growth while taking nutrient utilisation into consideration.

1.1. Review of related literature

Crop forecasting is crucial in agriculture because of soil and climatic elements, including temperature, humidity and rainfall. Due to the rapid changes in environmental conditions, farmers now find it difficult to keep cultivating. In recent times, machine-learning techniques, some of which have been used in research to compute agricultural production, have replaced traditional prediction tasks. To ensure a high level of accuracy, the data itself must be preprocessed using effective feature-selection methods to create a dataset that is easily calculable and machine-learning friendly. Appropriate choice of traits helps ensure that only the most relevant traits are incorporated into the model. The findings show that an ensemble approach performs better than existing classification approaches in precision [12].

Huang *et al.* [13], in a review, addressed the key distinctions and underlying relationships between several Bayes-theorem-based data-assimilation (DA) techniques. Building on that framework, the authors examined the development of various DA algorithms for assimilating data from crop models and remote sensing. DA has emerged as a key field of study for early-season crop-production forecasts over a wide area by combining the benefits of remote-sensing measurements and crop-growth models. Ntakos *et al.* [14] demonstrated how a crop-growth model may be parameterised using remote-sensing data, reducing the requirement for lengthy field measurements and taking crop-variety diversity into account while giving yield projections and crop-growth tracking. The study combined the state-rate World Food Studies (WOFOST) crop model with the Soil Canopy Observation of Photosynthesis and Energy (SCOPE) radiative-transfer model. The yield simulation produced encouraging results, with an average difference between measured and simulated values of 1800 kg/ha. The authors inferred that a coupled WOFOST–SCOPE model could enhance the use of remote-sensing data for crop-growth monitoring and yield prediction.

Gul *et al.* [2] used the Crop Environment Resource Synthesis (CERES) wheat model to demonstrate close agreement between observed and simulated grain-yield estimates. Annandale *et al.* [15] used the soil water balance model to set the values for growth features of 19 vegetable varieties, and field measurements were used to create a database of crop-development requirements. Zhao *et al.* [16] developed a generic crop model (SIMPLE) to simulate crop growth and yield. The model employs readily available inputs, such as daily weather data, crop management and soil water-holding parameters. It estimates biomass as a product of radiation, fraction of intercepted solar radiation, radiation-use efficiency, the effect of carbon dioxide (CO_2), the effect of temperature, heat stress and drought stress. The results showed an anticipated response of the model to gradual increments in temperature and CO_2. When compared with the Agricultural Systems Simulator (APSIM), Decision Support System for Agrotechnology Transfer (DSSAT) and WOFOST crop models, the SIMPLE model takes fewer input parameters, of which nine are species parameters and four are cultivar parameters. The low data requirements make it suitable for application to a wide range of crops. As a result of its simple nature, however, the model has limitations, including the absence of reaction to vernalisation and photoperiod effect on phenology. The model accounts for water utilisation but does

not take nutrient dynamics into consideration.

Many studies have used machine learning to forecast crop yield, with a focus on specific case studies. Paudel *et al.* [17] predicted yield for wheat, barley, sunflower, beetroot and potatoes by designing explainable predictors using machine learning (ML). Maimaitijiang *et al.* [18] evaluated the impact of data fusion using heat sensors and a deep neural network. The study improved prediction accuracy with a coefficient of determination (R^2) of 0.72. Sharifi [19] predicted barley yield based on remote-sensing and climate data using four machine-learning models, with Gaussian process regression performing best with an R^2 of 0.84. Huang *et al.* [13] predicted winter-wheat yield using multisource data and multiple ML models. The study projected support vector machine (SVM), Gaussian process regression and random forest as the best-performing models for predicting yield among the eight machine-learning models tested.

These days, much plant development takes place in greenhouses, and modern greenhouses enable the control of climatic conditions to guarantee maximum crop output. An essential precondition for effectively managing greenhouse factors is accurately predicting agricultural yields based on designated ecological factors. A new technique for forecasting greenhouse crop output was developed by combining the temporal convolutional network (TCN) and recurrent neural network (RNN) [20]. An improved soil-modelling system that integrates machine-learning techniques with evolving crop-growth information was proposed by Geng *et al.* [7]. Four practical settings were developed to determine the effect of crop-growth indicators as indicated by phenological metrics and the Normalised Difference Vegetation Index (NDVI). When compared with models that only used natural components, the results showed that adding time-series NDVI and phenological characteristics significantly improved model reliability, with predictions improving by as much as 36%.

Ahmed *et al.* [21] used NDVI and the chlorophyll green vegetation index (CI green VI) to predict winter-oat height and yield across three distinct phases of growth (flowering, grain filling and ripening) using a drone equipped with multispectral image sensors. Using the chemical indicators of crop quality and soil health, a logistic-regression machine-learning model was created to forecast oat yield. The authors concluded by outlining the range of soil nutrient concentrations and the crop-quality metric that growers need to maintain to maximise oat harvest yields.

Nitrogen remains the most limiting nutrient for crop development. The concept of the critical nitrogen dilution curve (CNDC) has been refined over time, with Zhou *et al.* [22] demonstrating that unified dilution curves can be created for irrigated corn. The merger of remote-sensing techniques has improved nitrogen-status assessment, with studies showing that drone imagery combined with ML methods can estimate nitrogen content accurately, with an R^2 of 0.77 for wheat [23]. Process-based crop models such as APSIM have been evaluated for their site-specific nitrogen-management capability, showing capacity to simulate maize-yield response to nitrogen with a relative root mean square error (RRMSE) of 12% [24]. Multiple-year prediction of the nitrogen nutrition index using UAV-based multisource remote sensing has achieved remarkable results, with the extremely randomised tree machine-learning model achieving an R^2 of 0.60 and a root mean square error (RMSE) of 0.14 for winter wheat, thus providing a strong argument for nitrogen management [25]. Crop-growth prediction remains a vital research problem in agriculture because researchers are focused on the prediction of yield, which remains the main interest of the farmer. Further research can be directed to developing models specifically for the prediction of not only yield but also the growth rate of crops as a function of above-ground biomass, while considering non-climatic growth factors such as nitrogen utilisation in the deployment of growth models [26].

Table 1: Description of input data.

SN	Description	Unit
1	All-sky surface PAR (radiation)	W/m^2
2	Daily maximum temperature (max_T)	°C
3	Daily minimum temperature (min_T)	°C
4	Atmospheric CO_2 concentration (CO_2)	ppm
5	Soil nitrogen (N)	g/kg
6	Plant-available water (PAW)	mm
7	Reference evapotranspiration (RETo)	mm

1.2. Motivation and contributions

Accurate prediction of crop biomass and yield under changing environmental conditions remains a major gap in agricultural modelling. Process-based crop-growth models such as that of Zhao *et al.* [16] have offered a useful framework for calculating biomass using environmental variables, but they have significant drawbacks that restrict their usefulness in practical applications. In particular, the Zhao model ignores soil–crop nutrient dynamics, especially nitrogen availability, which is essential for crop yield and biomass build-up. As a result, the model assumes optimal nutrient conditions and thus produces overestimated biomass predictions under nutrient-limited environments.

Therefore, this study develops an improved crop-biomass and yield-prediction framework that integrates soil nutrient dynamics into the biomass-estimation process to accurately represent vital crop physiological processes while utilising easily accessible environmental data such as remote-sensing and climate datasets. The contributions of the study are as follows:

1. generation of novel environmental data for cowpea, a regionally important but understudied crop, in Makurdi, Benue State, and Mokwa, Niger State, both in North Central Nigeria;
2. formulation of a model that incorporates nutrient utilisation for cowpea biomass prediction, with fewer parameters than existing models and with the ability to predict biomass accumulation of up to 175 kg/ha for the two study locations;
3. creation and testing of a novel hybrid architecture that shows a consistent performance increase with a prediction accuracy of 91.4% for the Makurdi test and 93.4%

Table 2: Description of parameters.

SN	Description	Parameter type	Calibration	Unit
1	Cumulative temperature requirement from sowing to maturity (Tsum)	Species	1200	°C
2	Cumulative temperature for leaf-area development at 50% radiation (ctLad)	Species	600	°C
3	Cumulative temperature for leaf senescence at 50% radiation (ctCS)	Species	600	°C
4	Base temperature for crop growth (base_T)	Species	10.0	°C
5	Optimal temperature required for biomass growth (opt_T)	Species	26	°C
6	Radiation-use efficiency (raduse_eff)	Species	0.82	g MJ^{-1} m^{-2}
7	Extreme temperature threshold at which raduse_eff is 0 (ext_T)	Species	38.0	°C
8	Increase in raduse_eff per ppm of elevated CO_2 (S_{CO2})	Species	0.07	g MJ^{-1} m^{-2}
9	Nitrogen	Soil	Makurdi (55), Mokwa (44)	g/kg
10	Plant-available water (PAW)	Soil	Makurdi (23), Mokwa (22)	mm
11	Threshold temperature (heat_T)	Species	28	°C
12	Sensitivity of raduse_eff to arid index (water_S)	Species	0.5	Dimensionless
13	Half-saturation point of nitrogen (NK)	Species	25	Dimensionless
14	Harvest index (HI)	Species	0.40	Dimensionless

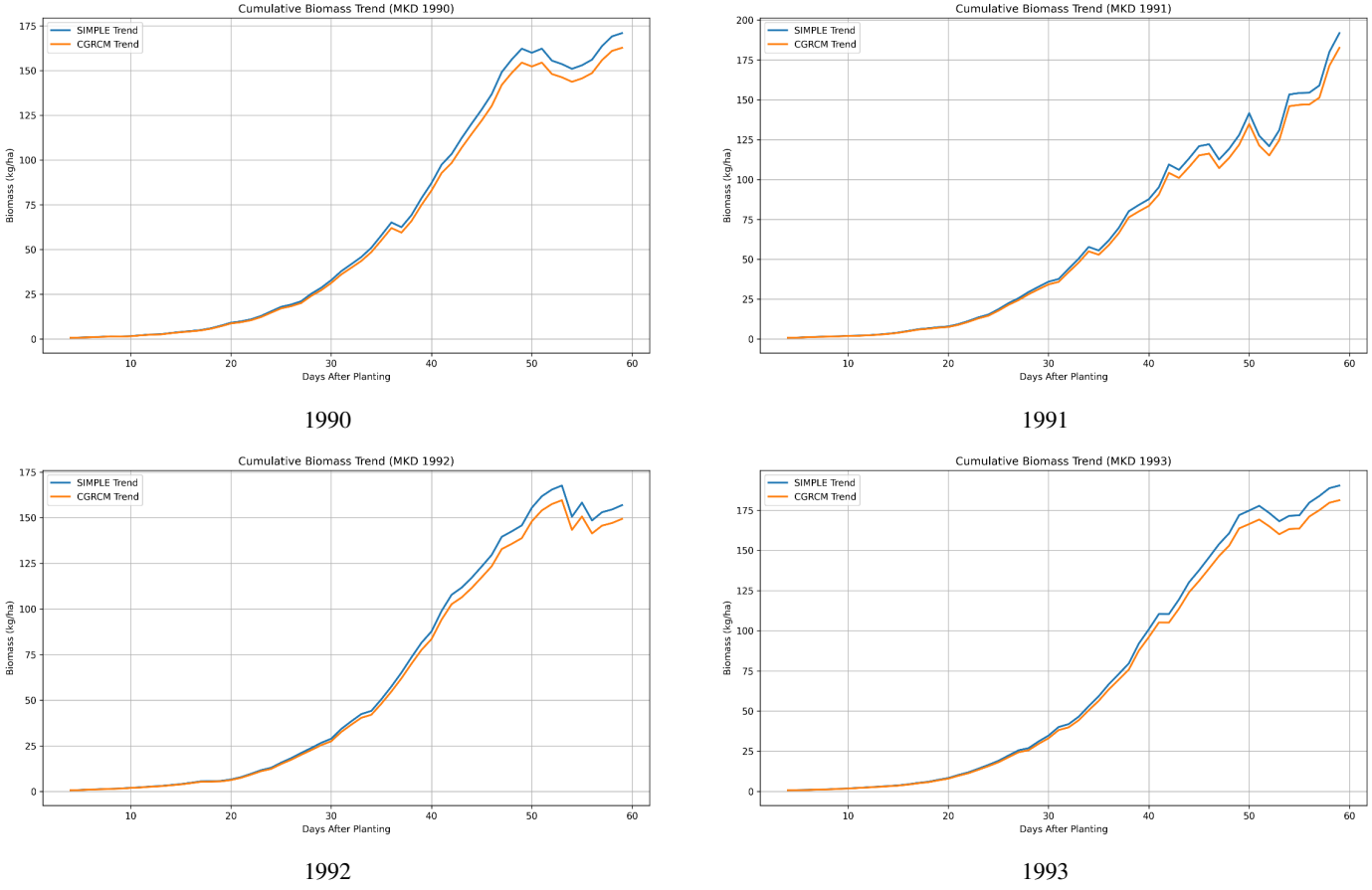

Figure 1: Cumulative biomass trend for Makurdi, 1990–1993.

Table 3: Algorithm of the proposed CGRCM.

Pre-condition: The CGRCM set is a dataset of radiation (rad), max_T, min_T, CO_2, N, PAW, RETo and DAP for the years 1990–2021, which are input data to CGRCM. The fields Tsum, ctLad, ctCS, base_T, opt_T, raduse_eff, ext_T, max_T and S_CO_2 are species parameters for the reference crop.
Post-condition: Steps 1–30 compute the cumulative biomass and yield for the reference crop.

Stage 1	**Calibration of parameters and data loading**
1	Calibrate Tsum, ctLad, ctCS, base_T, opt_T, raduse_eff, ext_T, max_T, harvest index (HI) and S_CO_2 with standard species-specific values.
2	Load climate data for training years (1990–2017).
3	Load observed yield data for evaluation years (2018–2021).
Stage 2	**Training-data preparation**
4	For each training year (1990–2017): (a) for each day after planting (DAP = 1 to end of season, approximately 62 days); (b) compute F_{CO2} according to equation (9); (c) compute N_{rad_eff} according to equation (13); (d) compute F_{sol} according to equation (4); (e) compute stress factors F_{temp}, F_{heat} and F_{water} according to equations (7), (8) and (10); (f) compute base biomass according to equation (14); (g) end for.
5	End for.
6	Compute seasonal_base_yield = cum_biomass × HI.
7	Compute target adjustment = average_observed_yield/seasonal_base_yield.
8	Save training data.
Stage 3	**Neural-network configuration and training data**
9	Initialise neural network with three inputs, three hidden layers (32, 16 and 8 neurons with rectified linear unit (ReLU) activation) and one linear output neuron.
10	Split data into training set (1990–2017) and validation set (2018–2021).
11	For epoch = 1 to 300.
12	Shuffle training samples.
13	For each batch of 32 samples.
14	Forward pass (using F_{temp}, F_{heat} and F_{water}) through all layers to get predicted adjustment.
15	Compute error = predicted adjustment – target adjustment.
16	Compute loss = error^2.
17	Compute gradient of loss in backward pass.

Table 4: Continuation of the algorithm of the proposed CGRCM.

Step	Algorithm continued
18	Update network parameters.
19	End for.
20	End for.
Stage 4	**Testing**
21	For test years, load daily climate data.
22	Set cum_biomass = 0.
23	Pass (F_{temp}, F_{heat}, F_{water}) through the trained network to obtain learned correction as Φ.
24	Compute final_biomass = base_biomass + Φ.
25	Set cum_biomass = cum_biomass + final_biomass.
26	End for.
27	Compute yield = cum_biomass × harvest index.
28	Compare predicted yield with observed yield for test years.
29	Compute error metrics.
30	Exit.

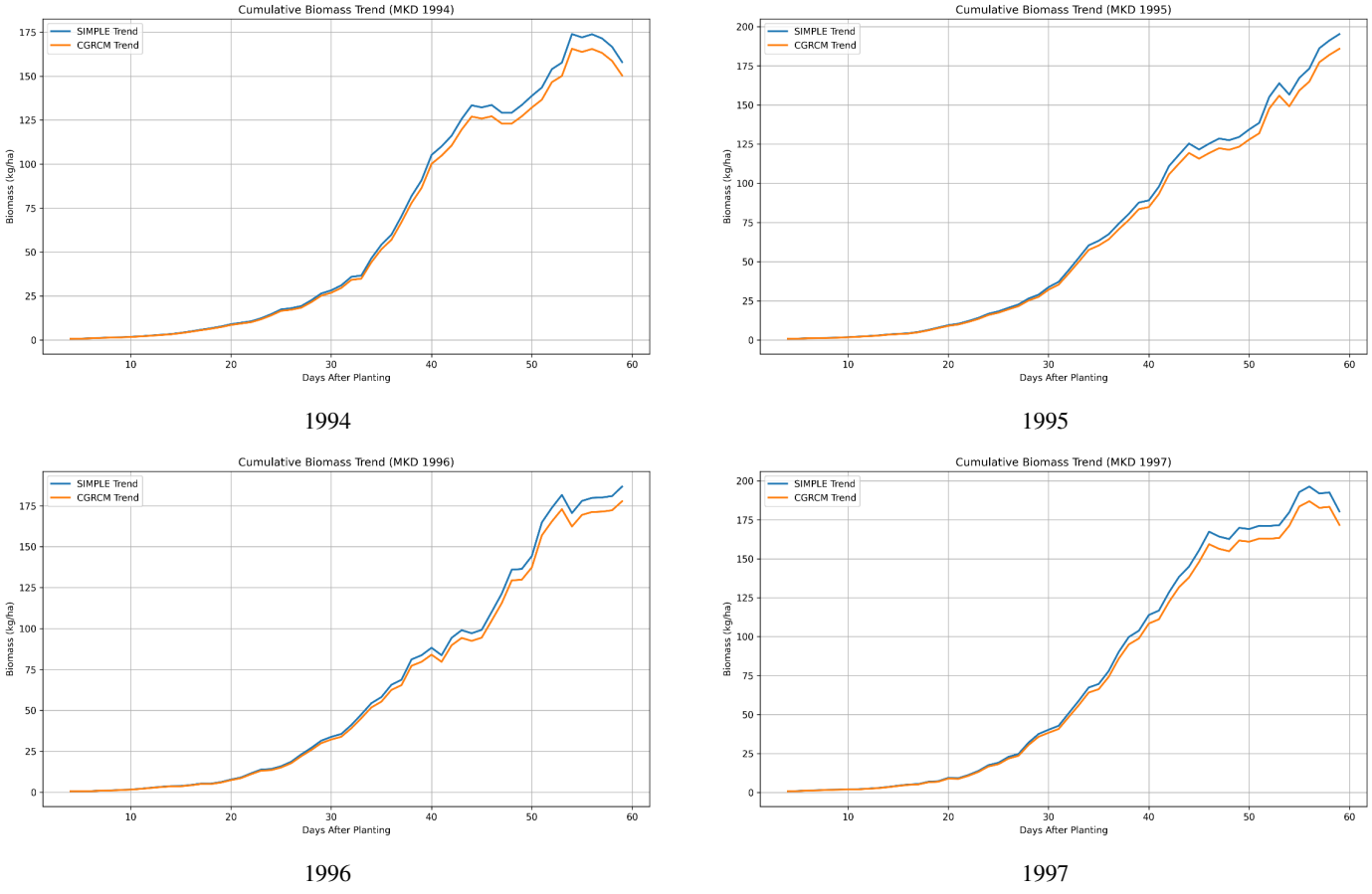

Figure 2: Cumulative biomass trend for Makurdi, 1994–1997.

Table 5: Performance evaluation of the CGRCM for Makurdi yield.

Model	MAE	RMSE	Prediction accuracy (%)
CGRCM	134.2	153.6	91.4
SIMPLE	196.6	311.0	81.0

Table 6: Performance evaluation of the CGRCM for Mokwa yield.

Model	MAE	RMSE	Prediction accuracy (%)
CGRCM	109.4	113.7	93.5
SIMPLE	167.3	172.4	90.2

for the Mokwa test by fusing process-based crop modelling with neural network learning;

4. provision of a reproducible framework that can be applied to other crops and geographic areas.

1.3. Outline of the work

This article is outlined as follows. The background of the research, review of related studies, research motivation and contributions are presented in Section 1. Section 2 presents the materials and methods, stating the source of data and study area, formulating the model equations and presenting the algorithm for the study. Section 3 presents the implementation results. Section 4 discusses the results and provides further insights into the significance of the contributions of this study. Section 5 presents the conclusion, including the background, the problem solved, the method used, the findings, the implications of the findings, the limitations of the study and suggestions for further research.

2. Materials and methods

2.1. Study area and data source

The reference crop for this study is cowpea, specifically the variety Federal University of Agriculture Makurdi PEA (FUAMPEA)–FUAM14122-17-7. The study focused on two selected sites: Mokwa and Makurdi towns, located at 9.2948°N, 5.0541°E and 7.733°N, 8.5158°E, respectively. Makurdi and Mokwa were selected because they are both located in the Guinea Savanna agro-ecological zone but exhibit differences in rainfall and temperature patterns. Makurdi has a mean annual rainfall of approximately 1200–1500 mm/year and a mean daily temperature of 26–28°C. Mokwa has a mean annual rainfall of approximately 1000–1300 mm/year and a mean daily temperature of 27–30°C.

Table 7: Statistical significance testing for CGRCM predictions.

Statistical test	Makurdi	Mokwa	Significance
Bootstrap CI (CGRCM RMSE)	118.6, 193.6 kg/ha	89.3, 141.2 kg/ha	Non-overlapping
Paired t-test	$t = 4.82$, $p = 0.017$	$t = 3.67$, $p = 0.035$	$p < 0.05$
Diebold–Mariano	DM = 2.34, $p = 0.028$	DM = 2.01, $p = 0.048$	$p < 0.05$
Cohen's effect size	$d = 1.92$ (large)	$d = 1.46$ (large)	Large effect

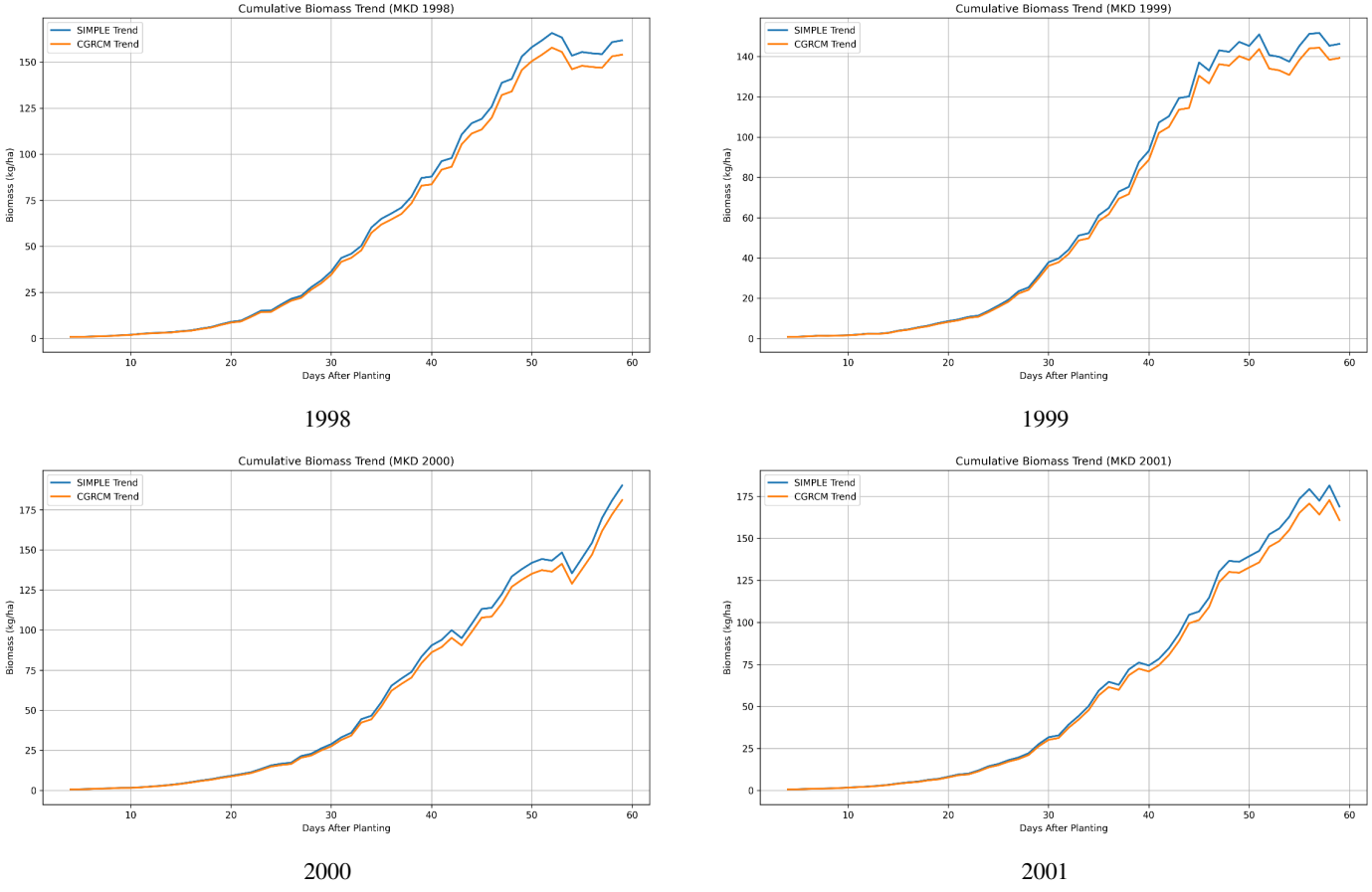

Figure 3: Cumulative biomass trend for Makurdi, 1998–2001.

The data for the study were obtained from remote sensing, and the analysis used a diverse dataset comprising daily and multi-year aggregated variables obtained from various authoritative sources. Data were obtained for a 62-day period from 15 August to 15 October, spanning 1990–2021, for Mokwa and Makurdi in North Central Nigeria. Precipitation data, measured in millimetres (mm), and all-sky surface photosynthetically active radiation (PAR), measured in watts per square metre (W/m^2), were sourced from NASA POWER [27]. Similarly, daily minimum and maximum temperature data at a 2-m height, recorded in degrees Celsius, were also obtained from the NASA POWER database [28]. Atmospheric CO_2 concentrations, reported in mol/mol and later converted to parts per million (ppm) for use in the model, were sourced from [29], providing daily temporal resolution. In addition to these daily datasets, soil nitrogen content (g/kg) and plant-available water (PAW, mm) were included as multi-year aggregate datasets. These data were derived from [30] and [31], respectively. Reference evapotranspiration (RETo), expressed in millimetres (mm), was incorporated from [33] on a daily temporal scale. The evapotranspiration, OCO-2, soil nitrogen content and plant-available water datasets were downloaded as spatial maps, and data variables for the study sites were extracted using ArcMap 10.3.1. The data utilised in this study are publicly available at [32].

2.2. *Description of input data and parameters*

The details of the input data and parameters for the study are presented in Tables 1 and 2.

2.3. *Description of the Crop Growth Rate Computation Model*

This study is based on the SIMPLE model by Zhao *et al.* [16], which models crop growth as a function of above-ground

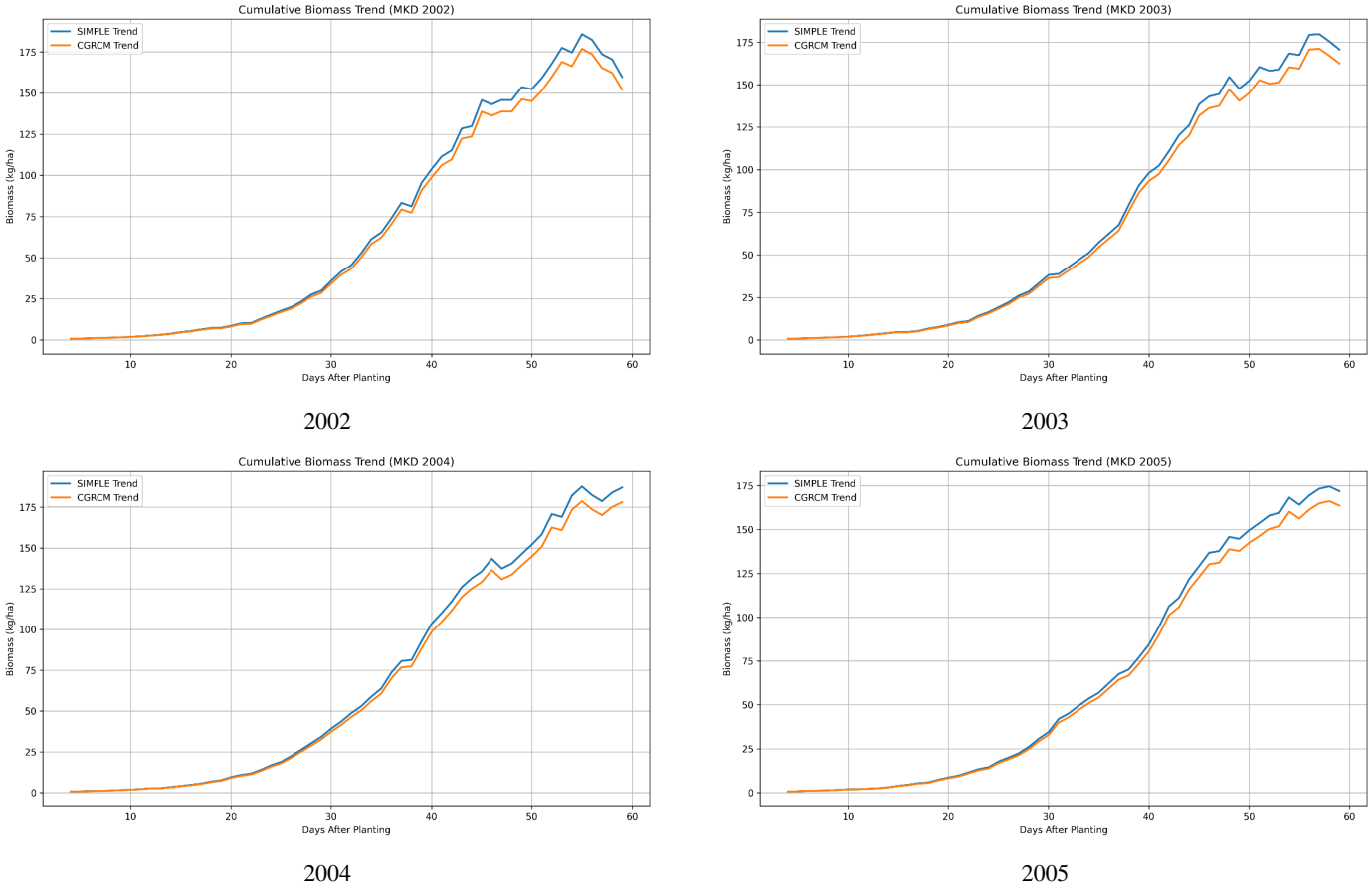

2002 2003

2004 2005

Figure 4: Cumulative biomass trend for Makurdi, 2002–2005.

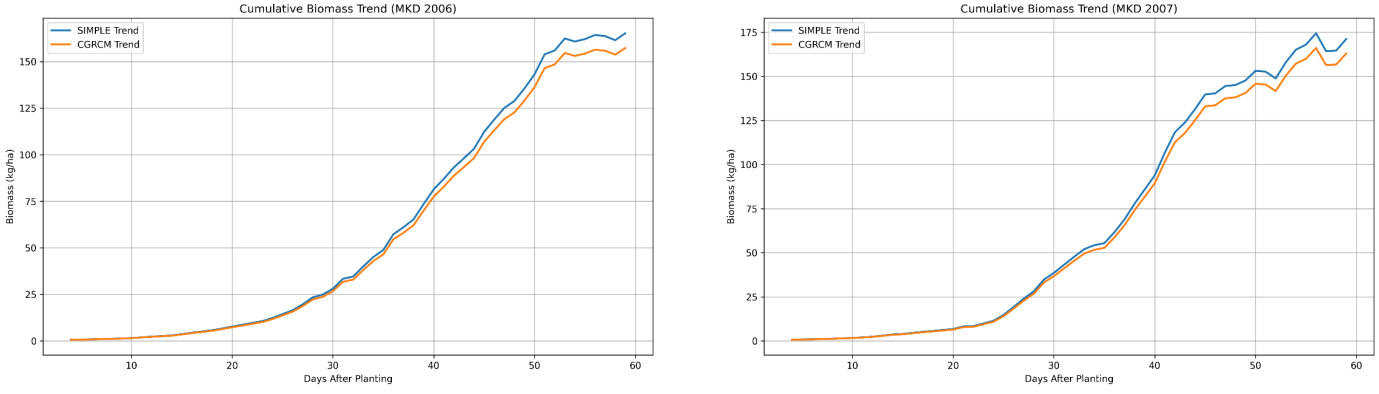

2006 2007

Figure 5: Cumulative biomass trend for Makurdi, 2006–2007.

biomass without taking nutrient-utilisation dynamics into consideration. The base model is given as:

$$\text{rate}_{\text{biomass}} = \text{Rad} \times F_{\text{sol}} \times \text{rad}_{\text{eff}} \times F_{\text{CO2}} \times F_{\text{temp}} \times \min(F_{\text{water}}, F_{\text{heat}}), \quad (1)$$

$$\text{cum\_biomass}_{i+1} = \text{cum\_biomass}_i + \text{rate}_{\text{biomass}}, \quad (2)$$

$$\text{final\_yield} = \text{cum\_biomass}_{\text{harvest}} \times HI, \quad (3)$$

where $\text{rate}_{\text{biomass}}$ is the biomass growth for each day, cum_biomass is the total biomass on a given day, final yield is the overall yield at maturity and HI is the harvest index.

F_{sol} is the percentage of solar energy taken in by the crop, rad_{eff} is the radiation-use efficiency of the species, F_{CO2} is the impact of CO_2, F_{temp} is the temperature impact, F_{heat} is the impact of heat and F_{water} is the drought impact. The fraction of

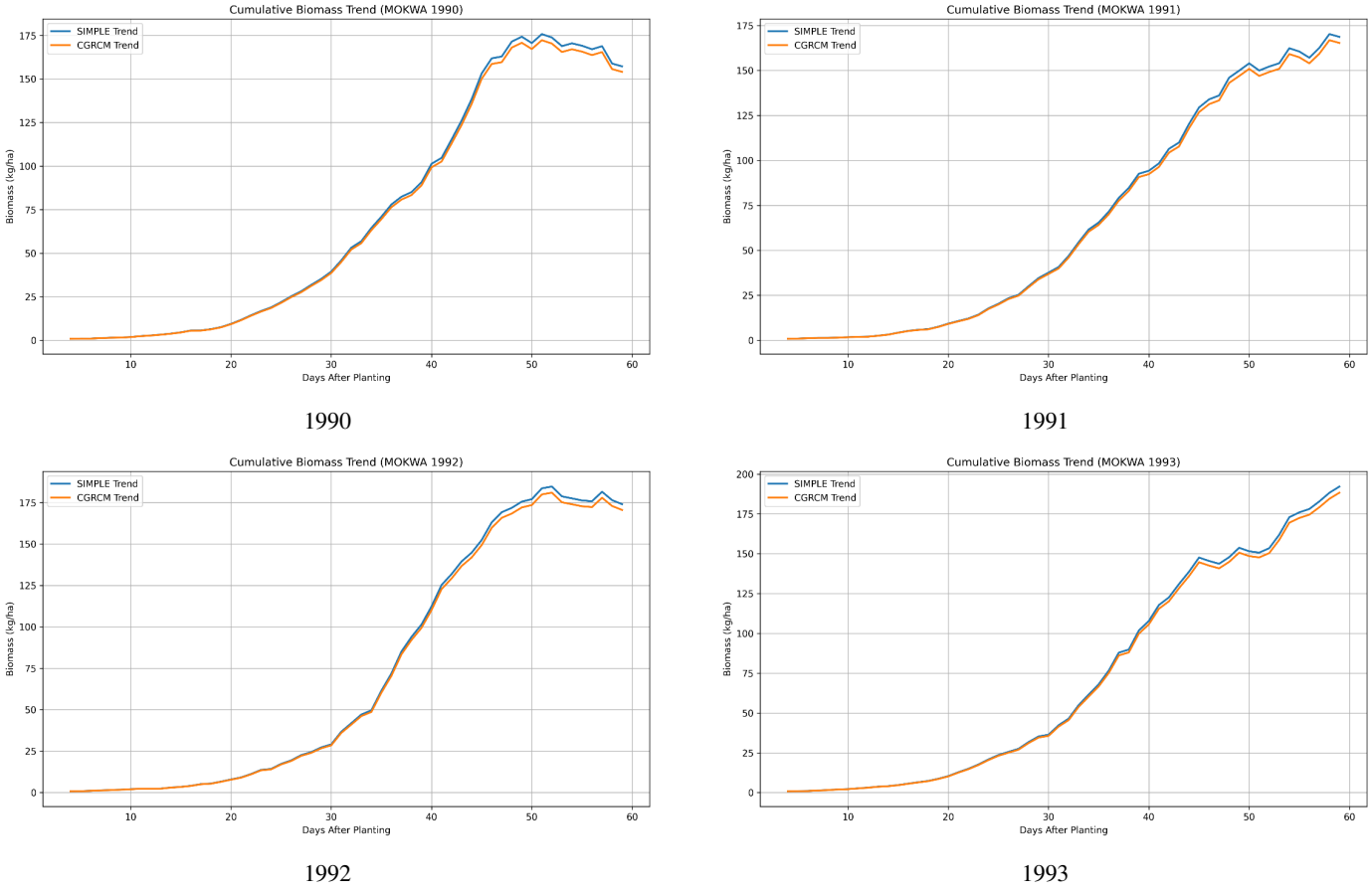

Figure 6: Cumulative biomass trend for Mokwa, 1990–1993.

solar radiation intercepted by the crop, F_{sol}, was obtained as:

$$F_{\text{sol}} = \begin{cases} \dfrac{F_{\text{sol\_max}}}{1 + e^{-0.01(\text{cmT} - \text{ctLAD})}}, & \text{leaf-growing,} \\ \dfrac{F_{\text{sol\_max}}}{1 + e^{0.01(\text{Tsum} - \text{ctCS})}}, & \text{leaf-senescence.} \end{cases} \tag{4}$$

where $F_{\text{sol\_max}}$ is the highest percentage of solar-energy absorption that a crop can attain.

The cumulative temperature (cmT) was obtained as:

$$\Delta\text{cmT} = \begin{cases} \text{Temp} - \text{base}_T, & \text{Temp} > \text{base}_T, \\ 0, & \text{Temp} \le \text{base}_T, \end{cases} \tag{5}$$

$$\text{cmT}_{i+1} = \text{cmT}_i + \Delta\text{cmT}, \tag{6}$$

where base_T is the base temperature for crop growth and cmT_i is the cumulative temperature on day i.

The impact of temperature on biomass growth (F_{temp}) was obtained as:

$$F_{\text{temp}} = \begin{cases} 0, & \text{dmt} < \text{base}_T, \\ \dfrac{\text{dmt} - \text{base}_T}{\text{opt}_T - \text{base}_T}, & \text{base}_T \le \text{dmt} < \text{opt}_T, \\ 1, & \text{dmt} \ge \text{opt}_T, \end{cases} \tag{7}$$

where dmt is the daily average temperature, and base_T and opt_T are the base temperature and optimal temperature for biomass increase for a specific crop.

The value for the heat impact (F_{heat}) on biomass growth is:

$$F_{\text{heat}} = \begin{cases} 1, & \text{max}_T \le \text{heat}_T, \\ 1 - \dfrac{\text{max}_T - \text{heat}_T}{\text{ext}_T - \text{heat}_T}, & \text{heat}_T < \text{max}_T \le \text{ext}_T, \\ 0, & \text{max}_T > \text{ext}_T. \end{cases} \tag{8}$$

where max_T is the maximum daily temperature, heat_T is the threshold temperature when heat starts depleting the rate at which biomass grows, and ext_T is the temperature when the growth rate of biomass reaches 0 owing to the impact of heat.

The impact of CO_2 (F_{CO2}) was obtained as:

$$F_{\text{CO2}} = \begin{cases} 1 + S_{\text{CO2}}(\text{CO}_2 - 350), & 350 \le \text{CO}_2 < 700 \text{ ppm}, \\ 1 + S_{\text{CO2}} \times 350, & \text{CO2} > 700 \text{ ppm}. \end{cases} \tag{9}$$

where S_{CO2} is the crop-specific sensitivity of rad_{eff} to high CO_2 level.

The drought impact (F_{water}) on biomass growth was obtained as:

$$F_{\text{water}} = 1 - \text{water}_S \times ARD, \tag{10}$$

where ARD is the aridity index and water_S is the sensitivity of rad_{eff} to the aridity index. ARD is obtained as:

$$ARD = 1 - \frac{\min(\text{RETo}, 0.096 \times \text{PAW})}{\text{RETo}}, \tag{11}$$

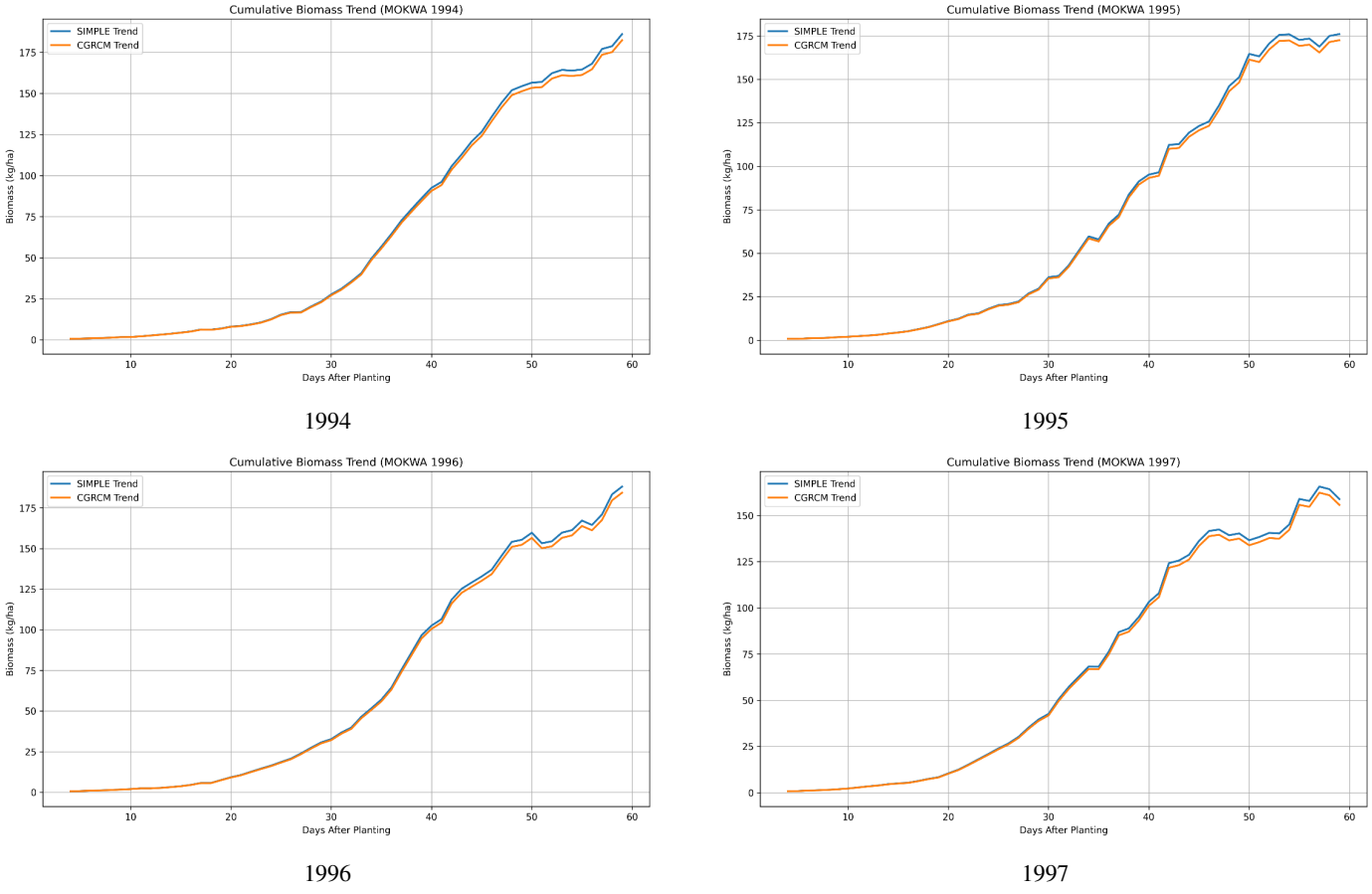

Figure 7: Cumulative biomass trend for Mokwa, 1994–1997.

where PAW is plant-available water.

Given that nitrogen availability in optimal quantity has a resultant impact on crop biomass, this study adopts a Michaelis–Menten-type equation from [34] for nitrogen uptake. The uptake of soil nitrogen is given as:

$$F_N = \frac{N}{N + NK}, \tag{12}$$

where NK is the half-saturation point of nitrogen. The impact of $f(N)$ on rad_{eff} is computed as:

$$N_{\text{rad\_eff}} = \text{rad}_{\text{eff}} \times f_N. \tag{13}$$

To account for the impact of nitrogen utilisation on biomass, equation (13) is substituted into equation (1) to give an improved biomass-computation model, the CGRCM, as:

$$\begin{aligned} \text{biomass}_{\text{imp}} = \text{Rad} \times F_{\text{sol}} \times N_{\text{rad\_eff}} \times F_{\text{CO}_2} \\ \times F_{\text{temp}} \times \min(F_{\text{water}}, F_{\text{heat}}). \end{aligned} \tag{14}$$

2.4. Algorithm of the proposed CGRCM

The algorithm for the study is data-driven and process-driven and is presented in Table 3. It is meant to predict biomass and seasonal yield. The algorithm initialises parameters such as temperature thresholds, radiation-use efficiency and harvest index and loads daily climate data for Makurdi and Mokwa. Using the model in equation (14), the algorithm partly determines the base biomass for each day of the planting season using values of solar radiation (Rad), canopy interception (F_{sol}), carbon dioxide (F_{CO2}) and the impact of nitrogen on radiation-use efficiency ($N_{\text{rad\_eff}}$). The algorithm uses computed values of temperature stress (F_{temp}), heat stress (F_{heat}) and water stress (F_{water}) for two functions. First, they are fed into a trained neural network that has already learnt the connection between patterns of environmental stress and variations in biomass production during a training phase (1990–2017). Over the course of the growing season, the final daily biomass values are added up to determine the total biomass, which is subsequently converted into seasonal yield using a predetermined harvest index. The trained neural network is applied to unknown data during the testing phase (2018–2021), and model performance is assessed using conventional metrics by comparing the projected yields with observed yields.

3. Results

The CGRCM was implemented in the Python programming language. A class named `ModelEquation` was defined with nine functions to compute cumulative temperature (cmT), fraction of solar radiation (F_{sol}), impact of temperature (F_{temp}), heat impact (F_{heat}), impact of CO_2 (F_{CO2}), drought impact (F_{water}),

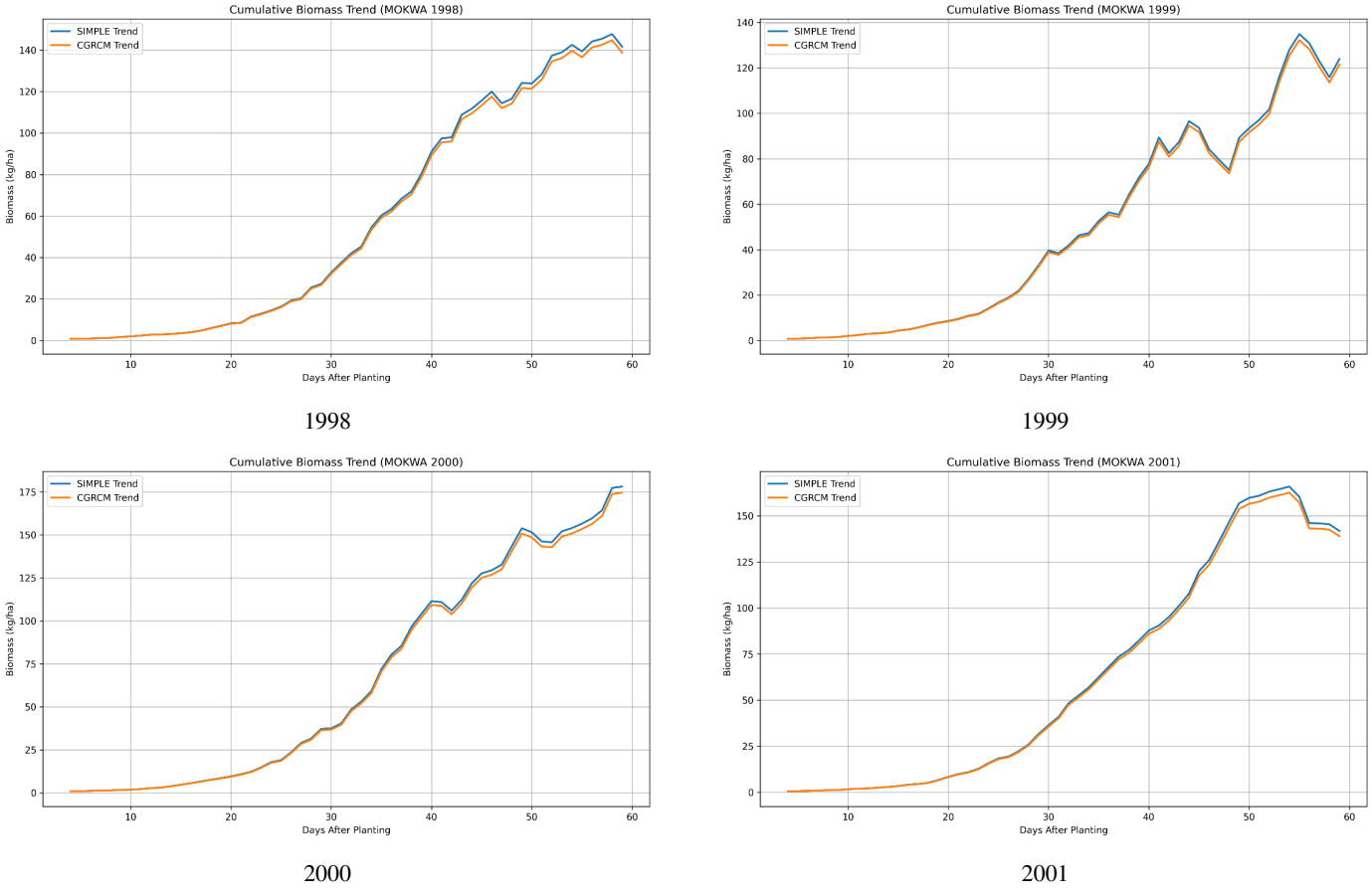

Figure 8: Cumulative biomass trend for Mokwa, 1998–2001.

aridity index and daily biomass rate (rate_biomass), each performing specific operations as specified in the algorithm in Section 2.4. The implementation includes a neural-network post-processor class that integrates a learned neural network with CGRCM. The network was trained on data from 1990 to 2017 for Makurdi and Mokwa, respectively, and tested on data from 2018 to 2021 for Makurdi and Mokwa, thus producing observed trends for FUAMPEA cumulative biomass and yield.

In Makurdi, North Central Nigeria, biomass production followed a radiation-dominated growth pattern with sigmoid-like trajectories in the growing seasons of 1990–1995 (Figures 1 and 2; Tables A1–A6, see Appendix). The primary factor that influenced biomass accumulation in every season was radiation interception (F_{sol}), which aided the change from early-stage growth limitations (DAP 1–20), mid-season growth (DAP 20–45) and late-season saturation (DAP 45–62). In the 1996–2001 growing seasons, the biomass rates showed a shift from early-stage growth limitation (DAP 1–20), which was marked by low F_{sol}, to a mid-season acceleration phase (DAP 20–45) (Figures 2 and 3; Tables A7–A12). Heat stress caused periodic late-season variation, but the temperature response remained stable in the timeframe. Together, the growing seasons of 2002–2007 (Figures 4 and 5; Tables A13–A18) show daily biomass accumulation shifts from early structural shortfalls (DAP 1–20), caused by low F_{sol}, to a prominent mid-season acceleration (DAP 25–45), which is driven by strong radiation-use efficiency. The 2008–2013 seasons (Figures A1 and A2; Tables A19–A24) featured late-stage stabilisation marked by rapid mid-season acceleration (DAP 25–45), driven by increases in F_{sol}, and slow development (DAP 1–20), caused by reduced canopy interception. Heat stress and few water fluctuations serve as temporal safeguards during this season while the temperature response is favourable. Biomass growth in the 2014–2019 seasons (Figures A3 and A4; Tables A25–A30) maintained late-season moderation reflecting physical saturation and stress balancing, and rapid mid-season expansion driven by F_{sol} increments (0.928–0.932). The 2020–2021 period (Figure A4; Tables A31–A32) saw a lower peak conversion efficiency due to temperature response, which is favourable but exhibits early-season inefficiency in comparison to mid-decade years. In contrast to heat dynamics, water stress acts as an extra control and stays contained within small ranges. With 2020 reaching 180 kg/ha and 2021 surpassing 185 kg/ha, the cumulative biomass curves show excellent seasonal performance, making 2021 one of the most productive years in the Makurdi dataset.

In the Mokwa experiment, an early development phase (DAP 1–20) hampered by limited canopy interception (F_{sol}), a rapid leafy expansion window (DAP 21–45) marked by gains in the efficiency of radiation capture, and a maturity phase (DAP 46–62) marked by peak biomass gains along with mild decline

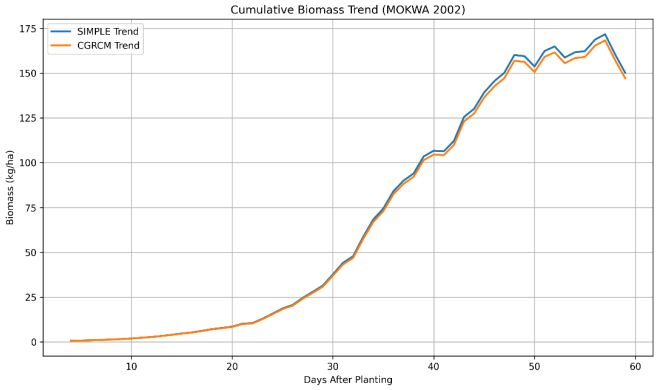

2002

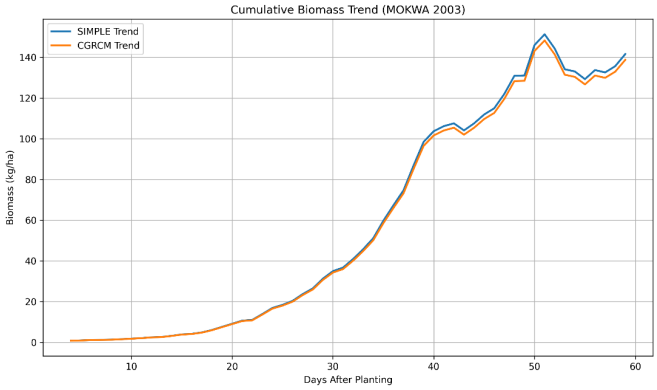

2003

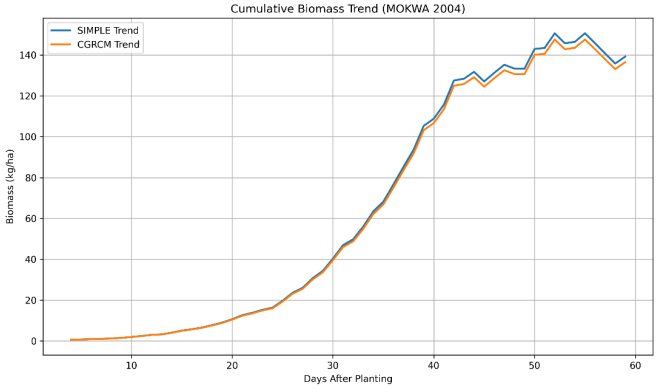

2004

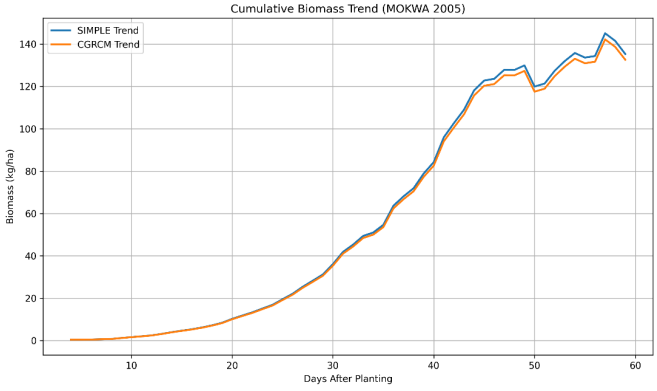

2005

Figure 9: Cumulative biomass trend for Mokwa, 2002–2005.

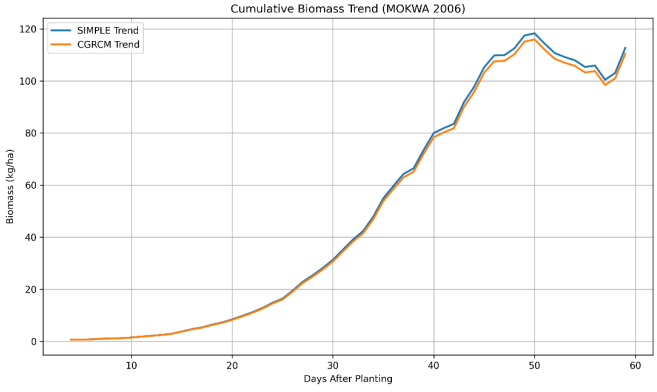

2006

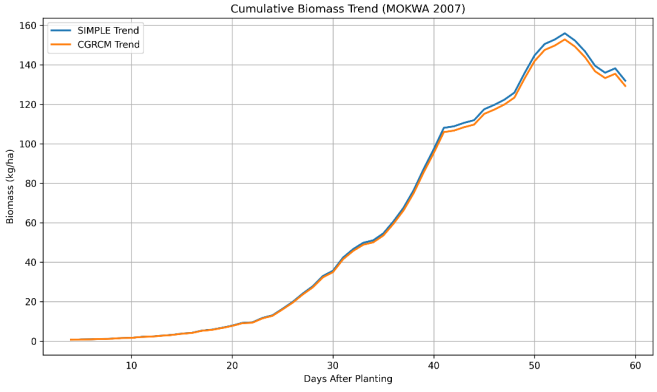

2007

Figure 10: Cumulative biomass trend for Mokwa, 2006–2007.

linked to thermal regulation are the hallmarks of the 1990–1995 biomass pathways (Figures 6 and 7; Tables A33–A38). The seasons of 1996–2001 (Figures 7 and 8; Tables A39–A45) demonstrate that different degrees of thermal and moisture control shaped late-season dynamics (DAP 46–62), mid-season expansion (DAP 21–45) was influenced by an increase in F_{sol}, and early growth (DAP 1–20) was affected by less canopy interception. Early growth (DAP 1–20) was reduced by incomplete canopy closure and low interception efficiency, according to the 2002–2007 predictions (Figures 9 and 10; Tables A46–A51). This was followed by a rapid vegetative acceleration window (DAP 30–48) that was closely timed with rising peak radiation-use efficiency. The 2008–2013 seasons (Figures A5 and A6; Tables A52–A57) show a productive and radiation-driven production cycle where cumulative paths maintained the sigmoidal architecture of tropical cowpea development. A steep leafy ex-

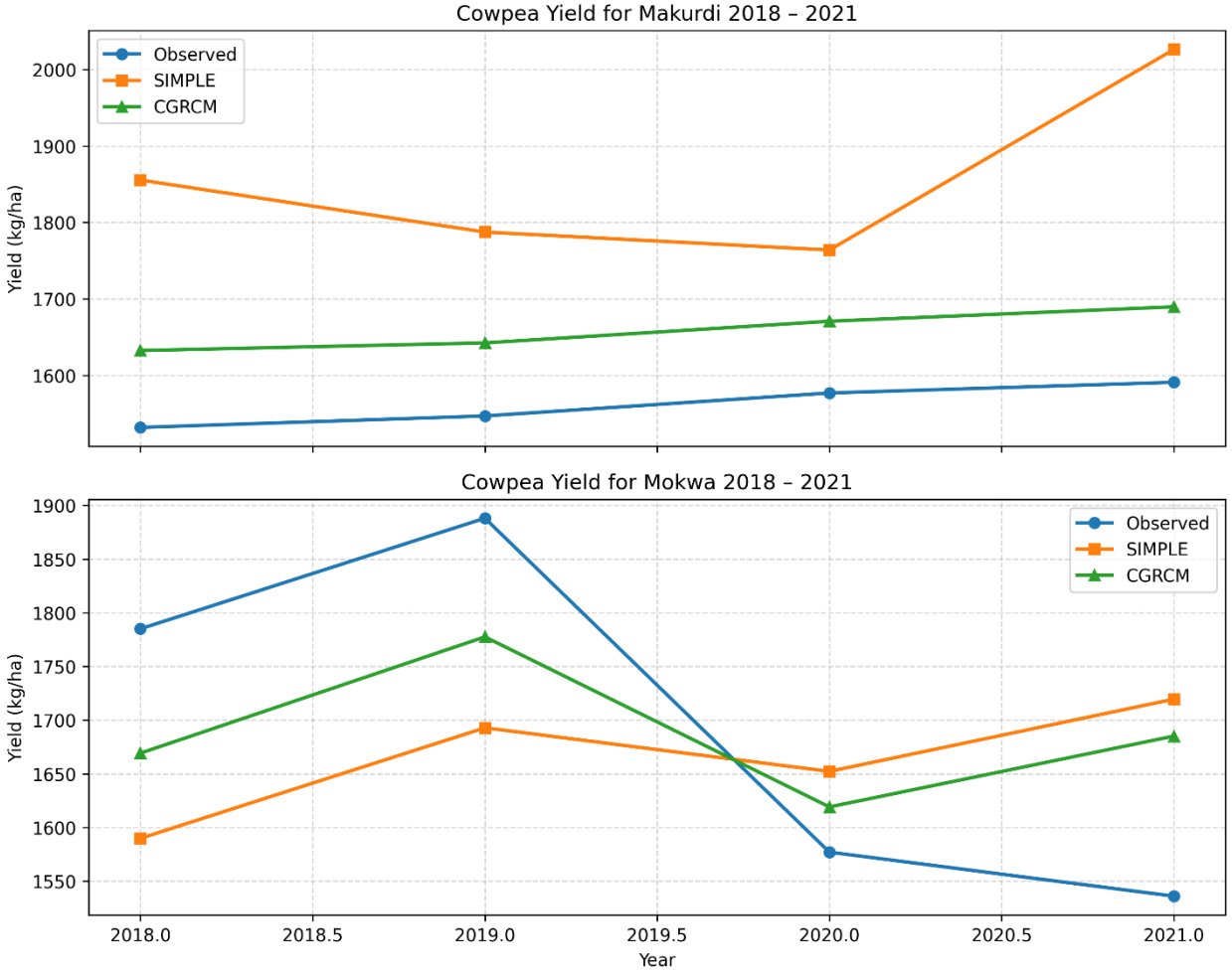

Figure 11: Cowpea yield trend for Makurdi and Mokwa, 2018–2021.

pansion timeframe characterised by rising F_{sol} (DAP 30–48), a maturity period shaped by heat and temperature-induced curvature, and an establishment phase limited by a decline in interception (DAP 1–20) are features of the 2014–2019 growing seasons (Figures A7 and A8; Tables A58–A63). With peak biomass values of approximately 156 kg/ha (2014), 175 kg/ha (2018) and 178 kg/ha (2019), the high-productivity years of 2014, 2018 and 2019 showed strong exponential growth periods that indicate optimum radiation capture and favourable water–heat balance. The results (Figure A8; Tables A64–A65) for 2020–2021 show that canopy radiation interception controls biomass ceilings and mid-season slope intensity, whereas thermal stress swings (F_{temp} and F_{heat}) are primarily responsible for late-season biomass stability.

The research was extended beyond growth-rate prediction as a function of above-ground biomass to include the prediction of final cowpea yield as a function of harvest index and cumulative biomass at maturity, as a way of validating the performance of CGRCM against observed yield data from [35] and predicted yield from SIMPLE. The model was trained on 3384 data points from Makurdi and Mokwa, respectively. A comparison of the observed yield and the CGRCM-predicted yield for the 2018–2021 validation period is shown in Figure 11, Tables A66 and A67. The CGRCM predictions show better agreement with observed yield values. With a mean absolute error (MAE) of 134.2, RMSE of 153.6 and prediction accuracy of 91.4%, compared to the SIMPLE model's MAE of 196.6, RMSE of 311.0 and accuracy of 81.0% for the test years 2018–2021, the Makurdi trend plot shows that the CGRCM generally produces more accurate yield predictions. In Mokwa, the CGRCM showed closer clustering to the observed yield, suggesting a closer match with observed yields. Therefore, the Mokwa yield trend plots support the Makurdi outcomes, demonstrating that the CGRCM improves prediction reliability with an MAE of 109.4, RMSE of 113.7 and prediction accuracy of 90.2%, compared to the SIMPLE model's MAE of 167.3, RMSE of 172.4 and prediction accuracy of 90.2% for the entire test period (2018–2021) across the two locations. The result of the evaluation of both models for both study locations is presented in Tables 5 and 6.

To ensure that the improvements from this study were statistically significant, three supplementary tests were conducted. First, bootstrap confidence intervals (CIs) for RMSE showed non-overlapping intervals between SIMPLE and CGRCM. For

Makurdi, SIMPLE's RMSE CI was 267–358 kg/ha, while CGRCM achieved 119–194 kg/ha. The absence of overlap means the difference is statistically significant. Second, a paired *t*-test on absolute percentage errors rejected the null hypothesis that both models perform equally. The *p*-values were 0.017 for Makurdi and 0.035 for Mokwa, both below the 0.05 threshold. Third, the Diebold–Mariano (DM) test, specifically designed for comparing forecast accuracy, produced *p*-values of 0.028 and 0.048, confirming that the CGRCM generates predictions that are significantly more accurate. Additionally, the Cohen's effect sizes were 1.92 and 1.46, with both considered large effects in statistical terms, meaning that the improvement is not only statistically significant but also practically meaningful. Together, these tests show that the CGRCM's outstanding performance is not accidental but represents a genuine improvement in prediction accuracy. A summary of the statistical tests carried out is presented in Table 7.

4. Discussion

Using a 32-year dataset covering 64 simulated growing seasons across two sites in Nigeria, Makurdi and Mokwa, both located in the North Central Guinea Savanna, this study assessed the predictive power of the CGRCM for the period 1990 to 2021. The findings show that important biological realism is introduced by the CGRCM formulation. The model incorporates an additional parameter that sets its hybrid architecture apart from the process-based core of the SIMPLE framework, which uses six main environmental response functions: temperature, heat, water, CO_2, radiation interception and radiation-use efficiency. Solar radiation interception (F_{sol}) was clearly the most important driver of biomass growth in all the 62 simulated growing seasons (31 years × 2 sites). In the majority of years, temperature responsiveness (F_{temp}) functioned as a permissive efficiency modulator rather than a primary limiter. Compared with temperature response, heat stress (F_{heat}) showed greater interannual variation, with notable late-season reduction occurring at both locations between DAP 45 and 60. Over the 32-year record, water stress (F_{water}) showed very little variation, with values between 0.50 and 0.60 and little daily variation.

Crop models that focus exclusively on maximising biomass accumulation often systematically overpredict yields because they fail to account for the complex interactions between stress factors and partitioning limitations. A model that predicts slightly lower biomass but with greater accuracy to observed yields provides more practical value for agricultural decision-making; hence, CGRCM stands out in this direction. The underlying premise of the SIMPLE model is that nitrogen is non-limiting. In contrast, nitrogen availability is explicitly included in the CGRCM as a dynamic variable that affects biomass accumulation and, eventually, grain yield. In tropical agricultural systems, where smallholder farmers typically lack access to synthetic fertilisers and must rely on organic inputs, biological nitrogen fixation and residual soil fertility, nitrogen is the most commonly limiting nutrient. In these situations, a model that disregards nitrogen dynamics is not only insufficient but also fundamentally incorrect. The CGRCM hybrid model's improved performance in all test years and locations, especially in the Makurdi and Mokwa environments, provides strong empirical support for the need to include nitrogen dynamics in crop models for agricultural systems in Sub-Saharan Africa.

5. Conclusion

Agriculture has sustained human civilisation for centuries, yet it remains a sector in critical need of technological advancement. Existing crop-growth and yield-prediction methods lack a simple and generic framework that relies on climate data with minimal parameters and nutrient-utilisation capabilities, particularly for leguminous crops. To solve this problem, this study developed an improved crop-biomass and yield-prediction framework that integrates soil nutrient dynamics into the biomass-estimation process to accurately represent vital crop physiological processes while utilising easily accessible environmental data such as remote-sensing and climate datasets. This was achieved by creating a hybrid crop-growth and yield-prediction framework that combines a neural network post-processor with a process-based CGRCM. The network was trained on data from 1990 to 2017 for Makurdi and Mokwa, respectively, and tested on data from 2018 to 2021 for Makurdi and Mokwa, thus producing observed trends for FUAMPEA biomass and yield. A comparison of the observed yield and the CGRCM-predicted yield for the 2018–2021 validation shows better agreement with observed yield values for both study locations.

The study shows that crop models that focus exclusively on increasing biomass estimates often systematically overpredict yield because they do not account for the complex interactions between stress factors and limiting conditions. A model that predicts slightly lower biomass but with greater accuracy to observed yields provides more practical value for agricultural decision-making; hence, CGRCM stands out in this direction. The limitation of this study is that it did not capture the impact of pest and disease dynamics on biomass accumulation. Future studies should include pest and disease factors in their growth-prediction models and also develop a user-friendly decision-support system with real-time data acquisition for practical deployment.

Data availability

The data utilised in this study are publicly available at [32].

Declaration of competing interest

The authors declare that they have no known competing financial interests or personal relationships that could have appeared to influence the work reported in this manuscript.

References

[1] J. James & M. Maheshwar, "Plant growth monitoring system, with dynamic user-interface", presented at 2016 IEEE Region 10 Humanitarian Technology Conference (R10-HTC). Available online: https://doi.org/10.1109/R10-HTC.2016.7906781.

[2] F. Gul, I. Ahmed, M. Ashfaq, D. Jan, S. Fahad, X. Li, D. Wang, M. Fahad, M. Fayyaz & S. A. Shah, "Use of crop growth model to simulate the impact of climate change on yield of various wheat cultivars under different agro-environmental conditions in Khyber Pakhtunkhwa, Pakistan", Arabian Journal of Geosciences **13** (2020) 112. https://doi.org/10.1007/s12517-020-5118-1.

[3] P. Patil, V. Panpatil & S. Kokate, "Crop prediction system using machine learning algorithms", International Research Journal of Engineering and Technology **7** (2020) 748. Available online: https://www.irjet.net/archives/V7/i2/IRJET-V7I2163.pdf.

[4] E. Elbasi, C. Zaki, A. E. Topcu, W. Abdelbaki, A. I. Zreikat, E. Cina, A. Shdefat & L. Saker, "Crop prediction model using machine learning algorithms", Applied Sciences **13** (2023) 9288. https://doi.org/10.3390/app13169288.

[5] H. Menon, D. Mishra & D. Deepa, "Automation and integration of growth monitoring in plants (with disease prediction) and crop prediction", Materials Today: Proceedings. Available online: https://doi.org/10.1016/j.matpr.2021.01.973.

[6] G. Worrall, A. Rangarajan & J. Judge, "Domain-guided machine learning for remotely sensed in-season crop growth estimation", Remote Sensing **13** (2021) 4605. https://doi.org/10.3390/rs13224605.

[7] J. Geng, Q. Tan, Y. Zhang, J. Lv, Y. Yu, H. Fang, Y. Guo & S. Cheng, "Leveraging remote sensing-derived dynamic crop growth information for improved soil property prediction in farmlands", Remote Sensing **16** (2024) 2371. https://doi.org/10.3390/rs16152731.

[8] P. Poudel, P. D. Alderman, T. E. Ochsner & R. P. Lollato, "A parsimonious Bayesian crop growth model for water-limited winter wheat", Computers and Electronics in Agriculture **217** (2024) 108618. https://doi.org/10.1016/j.compag.2024.108618.

[9] J. Li, L. Wang, J. Liu & J. Tang, "ViST: A ubiquitous model with multimodal fusion for crop growth prediction", ACM Transactions on Sensor Networks **20** (2023) 23. https://doi.org/10.1145/3627707.

[10] S. Kumar, G. Chowdhary, V. Udutalapally, D. Das & S. P. Mohanty, "GCrop: Internet-of-Leaf-Things (IoLT) for monitoring of the growth of crops in smart agriculture", presented at Proceedings–2019 IEEE International Symposium on Smart Electronic Systems, ISES. Available online: https://doi.ieeecomputersociety.org/10.1109/iSES47678.2019.00024.

[11] B. Grindstaff, M. E. Mabry, P. D. Blischak, M. Quinn & J. C. Pires, "Affordable remote monitoring of plant growth in facilities using Raspberry Pi computers", Applications in Plant Sciences **7** (2019) e11280. https://doi.org/10.1002/aps3.11280.

[12] S. P. Raja, B. Sawicka, Z. Stamenkovic & G. Mariammal, "Crop prediction based on characteristics of the agricultural environment using various feature selection techniques and classifiers", IEEE Access **10** (2022) 23625. https://doi.org/10.1109/ACCESS.2022.3154350.

[13] J. Huang, J. Song, H. Huang, W. Zhuo, Q. Niu, S. Wu, H. Ma & S. Liang, "Progress and perspectives in data assimilation algorithms for remote sensing and crop growth model", Science of Remote Sensing **10** (2024) 100146. https://doi.org/10.1016/j.srs.2024.100146.

[14] G. Ntakos, E. Prikaziuk, T. ten Den, P. Reidsma, N. Vilfan, T. van der Wal & C. van der Tol, "Coupled WOFOST and SCOPE model for remote sensing-based crop growth simulations", Computers and Electronics in Agriculture **225** (2024) 109238. https://www.wrc.org.za/mdocs-posts/watersa_2000_01_jan00_p67/.

[15] J. Annandale, N. Z. Jovanovic & J. G. Annandale, "Crop growth model parameters of 19 summer vegetable cultivars for use in mechanistic irrigation scheduling model", Water SA **26** (2000). Available online: https://www.researchgate.net/publication/267679732.

[16] C. Zhao, B. Liu, L. Xiao, G. Hoogenboom, K. J. Boote, B. T. Kassie, W. Pavan, V. Shelia, K. S. Kim, I. M. Hernandez-Ochoa, D. Wallach, C. H. Porter, C. O. Stockle, Y. Zhu & S. Asseng, "A SIMPLE crop model", European Journal of Agronomy **104** (2019) 97. https://doi.org/10.1016/j.eja.2019.01.009.

[17] D. Paudel, H. Boogaard, A. de Wit, S. Janssen, S. Osinga, C. Pylianidis & I. N. Athanasiadis, "Machine learning for large-scale crop yield forecasting", Agricultural Systems **187** (2021) 103016. https://doi.org/10.1016/j.agsy.2020.103016.

[18] M. Maimaitijiang, V. Sagan, P. Sidike, S. Hartling, F. Esposito & F. B. Fritschi, "Soybean yield prediction from UAV using multimodal data fusion and deep learning", Remote Sensing of Environment **237** (2020) 111599. https://doi.org/10.1016/j.rse.2019.111599.

[19] A. Sharifi, "Yield prediction with machine learning algorithms and satellite images", Journal of the Science of Food and Agriculture **101** (2021) 891. https://doi.org/10.1002/jsfa.10696.

[20] L. Gong, M. Yu, S. Jiang, V. Cutsuridis & S. Pearson, "Deep learning-based prediction on greenhouse crop yield combined TCN and RNN", Sensors **21** (2021) 4537. https://doi.org/10.3390/s21134537.

[21] S. Ahmed, N. Basu, C. E. Nicholson, S. R. Rutter, J. R. Marshall, J. J. Perry & J. R. Dean, "Use of machine learning for monitoring the growth stages of an agricultural crop", Sustainable Food Technology **2** (2024) 104. https://doi.org/10.1039/D3FB00101F.

[22] L. Zhou, B. Ming, K. Wang, D. Shen, L. Fang, H. Yang, J. Xue, R. Xie, P. Hou, J. Ye, J. Yu, T. Zhang, G. Zhang & S. Li, "Establishment of critical nitrogen-concentration dilution curves based on leaf area index and aboveground biomass for drip-irrigated spring maize in Northeast China", The Crop Journal **13** (2025) 556. https://doi.org/10.1016/j.cj.2025.01.009.

[23] A. M. Chegoonian, K. D. Singh, C. M. Geddes, C. Hansen & H. Wang, "Aerial insights: Advancing nitrogen estimation in field crops using multispectral imaging", International Archives of the Photogrammetry, Remote Sensing and Spatial Information Sciences **XLVIII-M-8-2025** (2025) 7. https://doi.org/10.5194/isprs-archives-XLVIII-M-8-2025-7-2025.

[24] H. Lei, F. Zhou, Q. Cai, X. Wang, L. Du, T. Lan, F. Kong & J. Yuan, "Effects of planting density and nitrogen management on light and nitrogen resource utilization efficiency and yield of summer maize in the Sichuan hilly region", Agronomy **14** (2024) 1470. https://doi.org/10.3390/agronomy14071470.

[25] D. Chen, Y. Chen, H. Zhang, J. Liu, Q. Cheng, F. Duan, X. Kuang, W. Fu, J. Liu & Z. Chen, "Diagnosis of nitrogen nutrition in winter wheat across years based on multi-source remote sensing data from unmanned aerial vehicles", Smart Agricultural Technology **12** (2025) 101481. https://doi.org/10.1016/j.atech.2025.101481.

[26] I. C. Onyeke, J. K. Alhassan, M. D. Abdulmalik & K. D. Tolorunse, "Development and challenges in intelligent prediction of crop growth: A systematic literature review", Proceedings of the 19th International Conference on Technology and Computing, Kano, Nigeria, 2025, p. 367. Available online.

[27] P. Stackhouse, "NASA POWER: Prediction of worldwide energy resources", NASA Langley Research Center, National Aeronautics and Space Administration. Available online: https://power.larc.nasa.gov/. Accessed November 2024.

[28] NASA, "NASA POWER Data Access Viewer: Daily meteorological data (2m minimum and maximum temperature)", NASA Langley Research Center, 2024. Available online: https://power.larc.nasa.gov/. Accessed November 2024.

[29] NASA Goddard Earth Sciences Data and Information Services Center (GES DISC), "Orbiting Carbon Observatory-2 (OCO-2) level 2 bias-corrected XCO_2, version 10r", NASA Goddard Space Flight Center, 2020. https://doi.org/10.5067/8E4VLCK16O6Q. Accessed November 2020.

[30] T. Hengl, M. A. E. Miller, J. Križan, K. D. Shepherd, A. Sila, M. Kilibarda, O. Antonijević, L. Glušica, A. Dobermann, S. M. Haefele, S. P. McGrath, G. E. Acquah, J. Collinson, L. Parente, M. Sheykhmousa, K. Saito, J. Johnson, J. Chamberlin, F. B. T. Silatsa & J. Crouch, "African soil properties and nutrients mapped at 30 m spatial resolution using two-scale ensemble machine learning", Scientific Reports **11** (2021) 6130. https://doi.org/10.1038/s41598-021-85639-y.

[31] ISRIC–World Soil Information, "SoilGrids: Global gridded soil information (soil nitrogen content and plant-available water layers)", 2024. Available online: https://soilgrids.org. Accessed 2 November 2024.

[32] I. C. Onyeke, J. K. Alhassan, A. D. Mohammed & K. D. Tolorunse, "Climate dataset for cowpea growth and yield prediction in North Central Nigeria", Zenodo, 2026. https://doi.org/10.5281/zenodo.19789732.

[33] Food and Agriculture Organization of the United Nations, "WaPOR database methodology: Version 2 release", FAO, Italy, 2020. Available

online: https://www.fao.org/3/ca9894en/CA9894EN.pdf.

[34] G. G. McNickle & J. S. Brown, "When Michaelis and Menten met Holling: Towards a mechanistic theory of plant nutrient foraging behaviour", AoB PLANTS **6** (2014) plu066. https://doi.org/10.1093/aobpla/plu066.

[35] L. O. Omoigui, A. Y. Kamara, A. S. Shaibu, K. T. Aliyu, A. I. Tofa, R. Solomon & O. J. Olasan, "Breeding cowpea for adaptation to intercropping for sustainable intensification in the Guinea Savannas of Nigeria", Agronomy **13** (2023) 1451. https://doi.org/10.3390/agronomy13061451.